OAK RIDGE NATIONAL LABORATORY
OPERATED BY
UNION CARBIDE CORPORATION
NUCLEAR DIVISION
POST OFFICE BOX X
OAK RIDGE, TENNESSEE 37831

Special Distribution
Limited to
Recipients Indicated

ORNL
CENTRAL FILES NUMBER
66-7-54

DATE: July 28, 1966

COPY NO. 85

SUBJECT: Comparison of the Results of Calculations Done at Different Laboratories with Each Other and with Experiments on the Secondary Proton and Neutron Spectra from Protons at 140 and 160 MeV on Nuclei

TO: Listed Distribution

FROM: H. W. Bertini, Neutron Physics Division

ABSTRACT

Comparisons are illustrated between calculations which were done by various groups. These groups are located at the Oak Ridge National Laboratory, at Los Alamos, and in the Brookhaven area. Experimental data are included with each comparison. The data being considered are those parts of the secondary proton and neutron spectra that lie above about 20 MeV and that are measured at various angles. The interactions are 140- and 160-MeV protons on several elements ranging from aluminum to bismuth. The calculation that differs most from experimental results is probably the Brookhaven calculation, which is the latest and most detailed. The differences are apparently due to the inclusion of reflection and refraction effects in the calculation. When these effects are not included, the results from the calculations of all three groups are very similar.

COMPARISON OF THE RESULTS OF CALCULATIONS DONE AT DIFFERENT LABORATORIES WITH EACH OTHER AND WITH EXPERIMENTS ON THE SECONDARY PROTON AND NEUTRON SPECTRA FROM PROTONS AT 140 AND 160 MeV ON NUCLEI

I. INTRODUCTION

This memorandum is intended to illustrate the results of calculations performed by different groups on the secondary particle spectra from 140- and 160-MeV protons incident on various elements. The data from the Brookhaven and Los Alamos groups are preliminary in nature and were kindly sent to the author at his request.

All of the calculations are of the same general type, i.e., Monte-Carlo cascade calculations. They differ in the assumptions each makes about the properties of the nucleus which is being bombarded. There is also a difference in the sampling technique which is used to determine the collision points and the types of particle-particle reactions that occur within the nucleus for each cascade particle. The free particle cross sections that were used in each calculation are essentially the same.

II. ORNL CALCULATION

The details of the author's calculations done at ORNL are given in reference 1. Briefly, the nucleus is assumed to be made up of three concentric spheres, i.e., a central sphere and two surrounding spherical annuli. The proton density within each sphere is constant, but it decreases from sphere to sphere as one goes from the inside to the outside. This density distribution is made to approximate the Fermi-type continuous charge distribution of Hofstadter.[2] The spherical boundaries apply to the neutrons as well as the protons, and the neutron to proton density in each region is the same as the neutron to proton ratio in the nucleus. The densities are such that if one takes the sum over the three regions of the product of density times volume in each region the sum will equal the atomic number or the neutron number of the nucleus.

Associated with each region there is a negative potential for the protons and one for the neutrons to account for the nuclear forces. The depth of the well for each region is equal to the sum of the zero temperature Fermi energy (calculated from the neutron or proton density) plus a binding energy. The binding energy is arbitrarily assumed to be the same for each region and for both protons and neutrons, and it is the same for all nuclei. As an incident particle passes from one region to another, its kinetic energy increases or decreases as the well depth increases or decreases. The bound nucleons within the nucleus in each region are assumed to have the zero temperature Fermi Energy distribution appropriate to that region.

The cut off energy of the cascade calculation, i.e., the energy below which the particle histories are no longer followed inside the nucleus, is arbitrarily assumed to be the depth of the potential of the region in which the particle is located (neutron potential for cascade neutrons and proton potential for cascade protons) plus one-half the coulomb potential at the surface of the nucleus.*

As the cascade reaction progresses the depletion of the nucleus is not taken into account.

The sampling technique that is used is described in detail elsewhere.[3] Very briefly, it consists of first estimating a maximum macroscopic cross section for the region. Then a distance of travel, a struck particle, and a type of reaction are selected using this cross section along with

---

*It should be realized that the outer radius of each nucleus is <u>not</u> determined by $r = (1.3F)A^{1/3}$ but is the radius at which the continuous charge distribution function[2] reaches 0.01 of its density at $r = 0$.

appropriate sampling and rejection techniques. Since one has chosen a maximum cross section (minimum mean free path) one rejects and selects another distance of travel successively (each distance is added to the sum of the first distance and the other distances selected) and often enough so that the correct mean free path is selected, on the average. This sampling technique is exact, i.e., it samples correctly from the proper distribution functions.

The procedure is fairly complicated because variables not normally encountered in ordinary transport calculations are introduced by the fact that the struck nucleons are in motion. For example the center of mass energy changes significantly when a cascade particle strikes a bound nucleon whose momentum vector is antiparallel to that of the cascade particle as opposed to that when the cascade particle strikes one whose momentum vector is parallel. Hence, the cross sections for all of the possible reactions are dependent on the vector momentum of the struck particle, and so is the reaction rate. In addition to this the expressions must take relativistic effects into account.

Reflection and refraction effects are not included.

III. BROOKHAVEN CALCULATION

The calculation being done by a group located in the Brookhaven area differs from the ORNL calculation in the following respects:

There are seven spherical regions instead of three, where the density distribution is again made to approximate Hofstadters Fermi-type charge distribution.[2]

There is a neutron and proton negative potential for each region as before. The depth of the well in each region is calculated to be the sum

of a zero temperature Fermi energy plus a binding energy which is the same for each region, but in this case the binding energy varies from nucleus to nucleus.

The cut off energy for neutrons in any region is the neutron Fermi energy in that region plus twice the binding energy. The cut off energy for protons is either the proton Fermi energy plus twice the binding energy or the proton Fermi energy plus the binding energy plus the coulomb potential at the nuclear surface, whichever sum is larger.

Nuclear depletion is not taken into account.

The sampling technique is exact, and it traces the cascade histories in time rather than space.

The most significant change, however, is that this calculation attempts to account for reflection and refraction effects as the cascade particles cross the region boundaries.

The energy distribution of the bound nucleons is the same as the ORNL calculation.

The people associated with this calculation are Catherine Chen (Columbia University), Z. Fraenkel (Wiesmann Institute, Israel), G. Friedlander (Brookhaven), J. R. Grover (Brookhaven), J. M. Miller (Columbia University), and Y. Shimamoto (Brookhaven).

IV. LOS ALAMOS CALCULATION

The calculation of the Los Alamos group includes the following assumptions:

The density distribution of the nucleons inside the nucleus is assumed to be the same as Hofstadters Fermi-type charge distribution,[2] but in determining the point of collision along a particular trajectory, the average

cross section along that trajectory is used first in calculating the probability of collision inside the nucleus. When it is decided that a collision will occur, the trajectory is broken up into segments that are 0.1F in length, an average density is calculated for each length, and then using these average densities the collision point within one of these segments is determined.

There is a negative potential associated with the nucleus, but it is assumed to be constant throughout the nucleus. Its magnitude is the same as that of the earlier work of Metropolis et al.,[4] i.e., the well depth is the sum of a zero temperature Fermi energy and a binding energy. The zero-temperature Fermi energy is calculated from the density of a nucleus which is assumed to be constant where the nuclear radius is given by $r = (1.3F) \times A^{1/3}$. The binding energy varies with the nucleus.[4]

The energy distribution of the bound nucleons is assumed to that given by the zero-temperature Fermi distribution just mentioned.

The cut off energy for protons is the well depth for protons plus the coulomb potential at the surface of the nucleus with a radius of $r = (1.3F) \times A^{1/3}$. The cut off energy for neutrons is the same as for protons, but since the neutron energy is measured from the bottom of the neutron well, and this well is usually deeper than the proton well, the neutrons can usually escape with smaller energies than the protons.

Nuclear depletion is not taken into account.

The sampling technique that is used to determine the distance of travel is described above. The selection of the type of reaction is based on the macroscopic cross sections, and the struck particle is selected from a

Fermi-momentum distribution which is isotropic in momentum space.* This overall selection procedure is an approximation to those used by ORNL and the Brookhaven groups.

Reflection and refraction effects are not considered.

The men doing the bulk of the work are Donald R. Cochran, John Wooten, and Robert Bivins, all of Los Alamos.

V. COMPARISONS OF THE CALCULATED SPECTRA WITH EACH OTHER AND WITH EXPERIMENT

The neutron spectra in the forward direction from 143-MeV protons on aluminum and lead are illustrated in Figs. 1 and 2, where the ORNL and Brookhaven calculations are shown along with the experimental data of Bowen et al.[5] Neither calculation does too well in comparing with the experiment. There is illustrated in Fig. 2 a rather typical result from the Brookhaven calculation, and that is that the inclusion of reflection and refraction effects in the calculation suppresses the "quasi-elastic" peak for heavier target nuclei.

Figs. 3-6 contain comparisons between the ORNL and Los Alamos calculations and the experiments of Roos and Wall[6] for the secondary protons emitted at various angles from 160-MeV protons on beryllium.

The calculations give somewhat different results at 20° and 40°, but are essentially the same at the wider angles. Of the two, the Los Alamos results compare more favorably with the experimental data.

---

*D. R. Cochran of Los Alamos was not sure about the isotropy. It had been a long time since he has worked on the code when he was asked about it over the phone. An anistropic distribution of struck particles may be used in order to account for the energy dependence of the cross sections as was done by Metropolis et al.[4]

Fig. 1. Secondary neutron spectrum at 2.5° from 143-MeV protons on aluminum. Solid-line curve: experimental spectrum of Bowen et al. (Ref. 5); circles: calculated data of the Brookhaven group for neutrons emitted in the angular interval 0 - 8° where reflection and refraction are included in the calculation; solid-line histogram: calculated spectrum of the ORNL group for neutrons emitted in the angular interval 0 - 5° from 140-MeV incident protons.

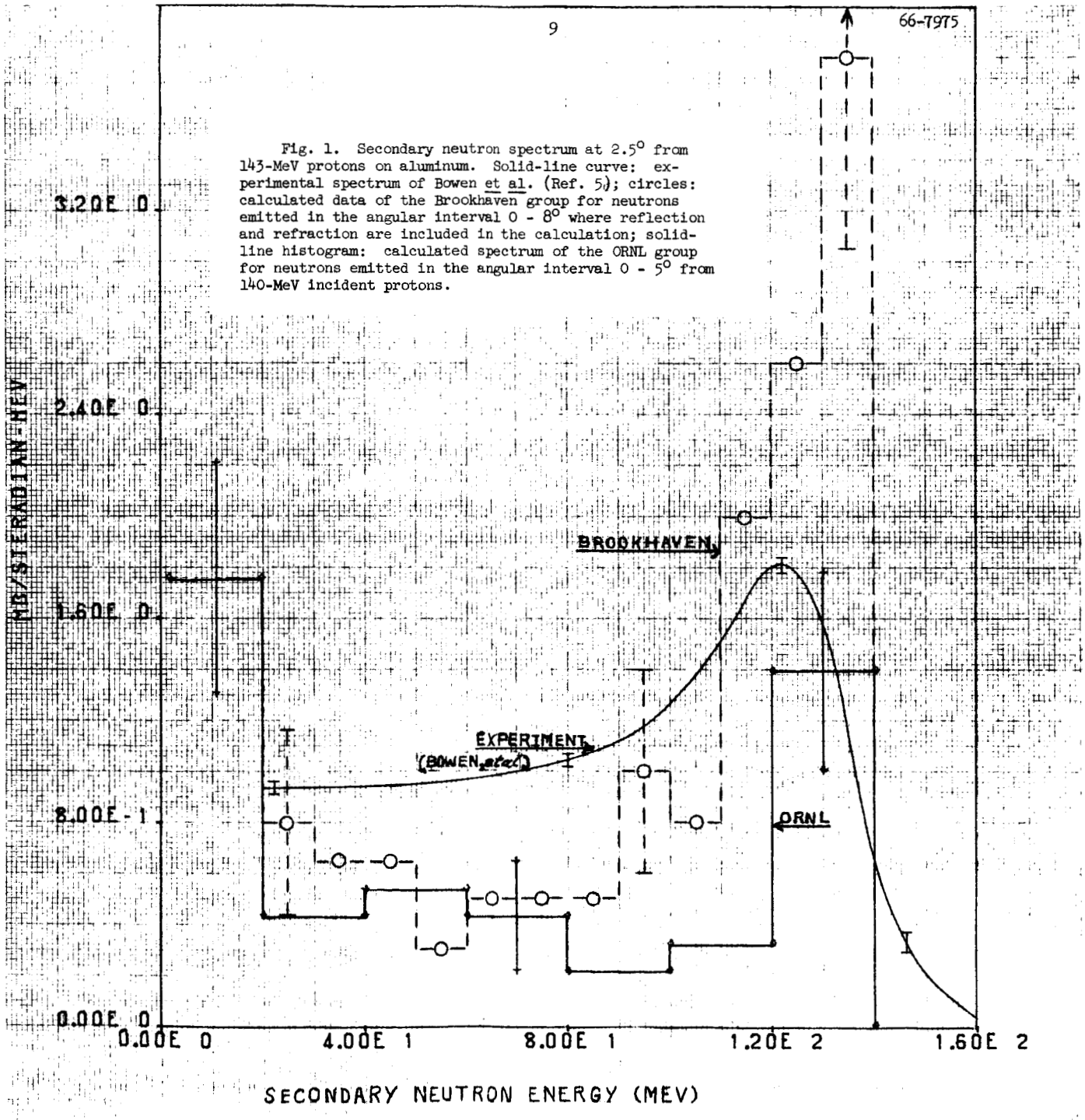

Fig. 2. Secondary neutron spectrum at 2.5° from 143-MeV protons on lead. Solid-line curve: experimental spectrum of Bowen et al. (Ref. 5); circles: calculated data of the Brookhaven group for neutrons emitted in the angular interval 0 - 8° where reflection and refraction are included in the calculation; solid-line histogram: calculated spectrum of the ORNL group for neutrons emitted in the angular interval 0 - 5° from 140-MeV incident protons.

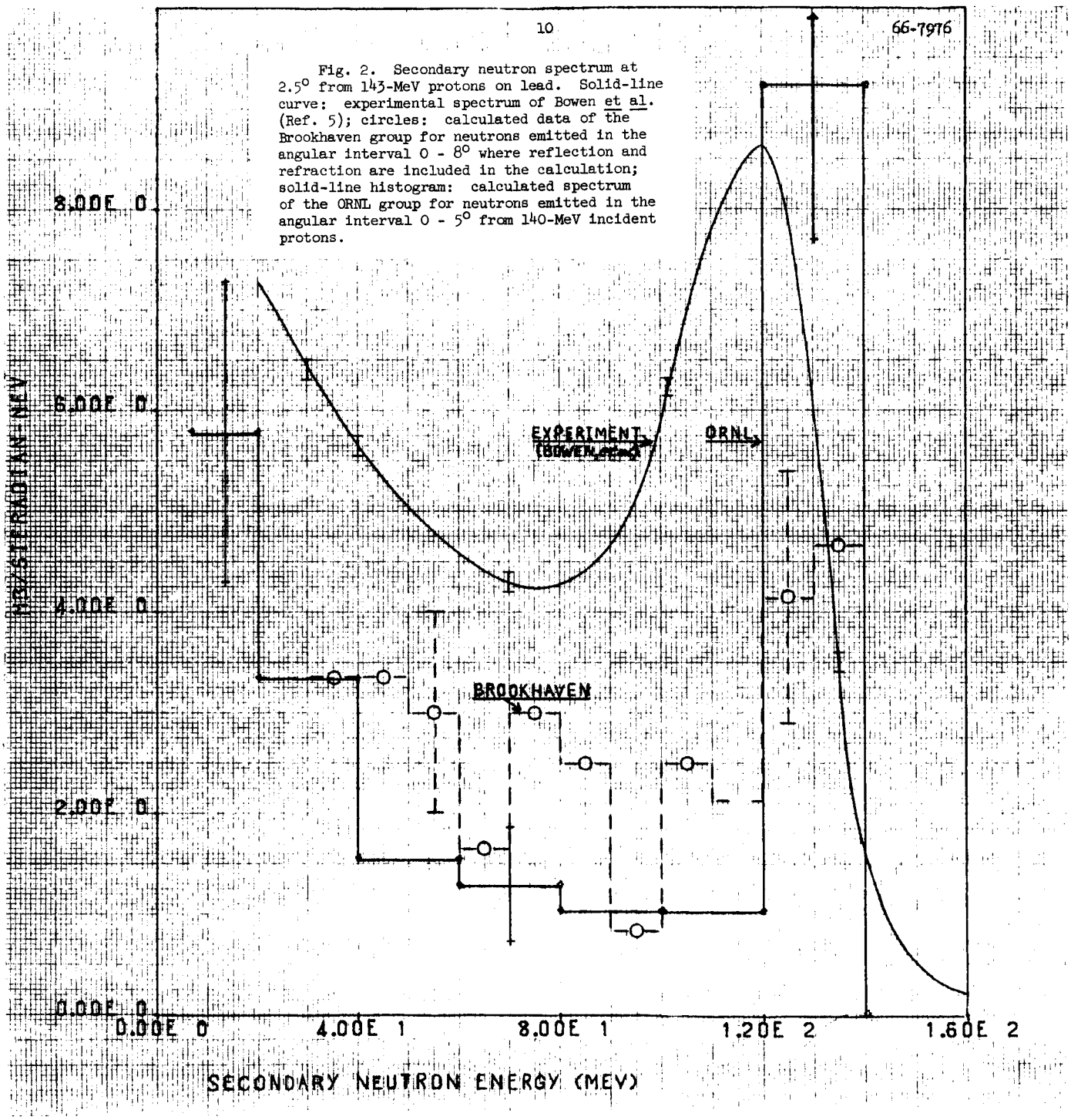

Fig. 3. Secondary proton spectrum at 20° from 160-MeV protons on beryllium. Solid-line curve: experimental spectrum of Roos and Wall (Ref. 6); squares: calculated data of the Los Alamos group for protons emitted in the angular interval 18 - 22°; solid-line histogram: calculated spectrum of the ORNL group for protons emitted in the angular interval 15 - 25°.

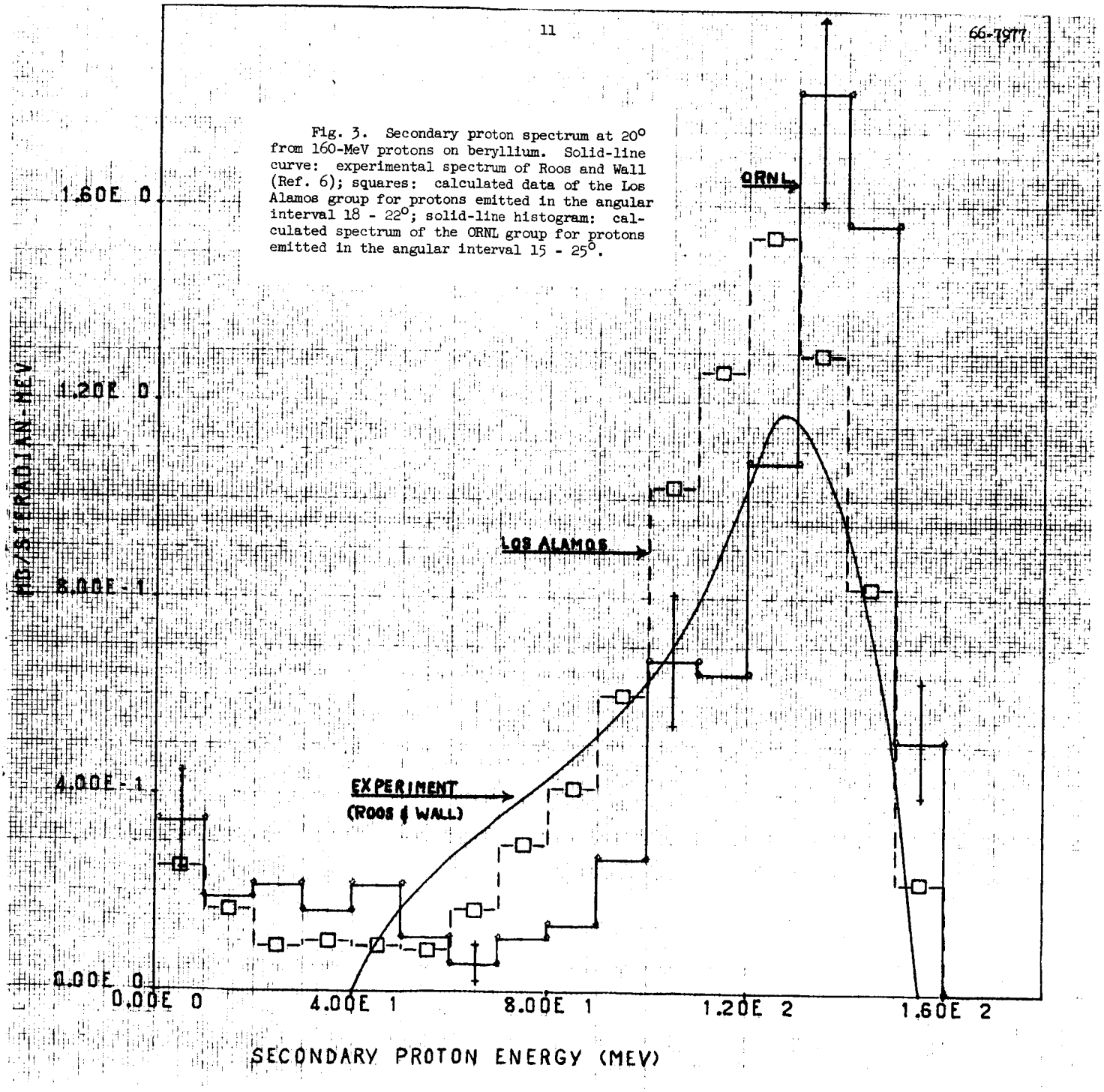

Fig. 4. Secondary proton spectrum at 40° from 160-MeV protons on beryllium. Solid-line curve: experimental spectrum of Roos and Wall (Ref. 6); squares: calculated data of the Los Alamos group for protons emitted in the angular interval 38 - 42°; solid-line histogram: calculated spectrum of the ORNL group for protons emitted in the angular interval 35 - 45°.

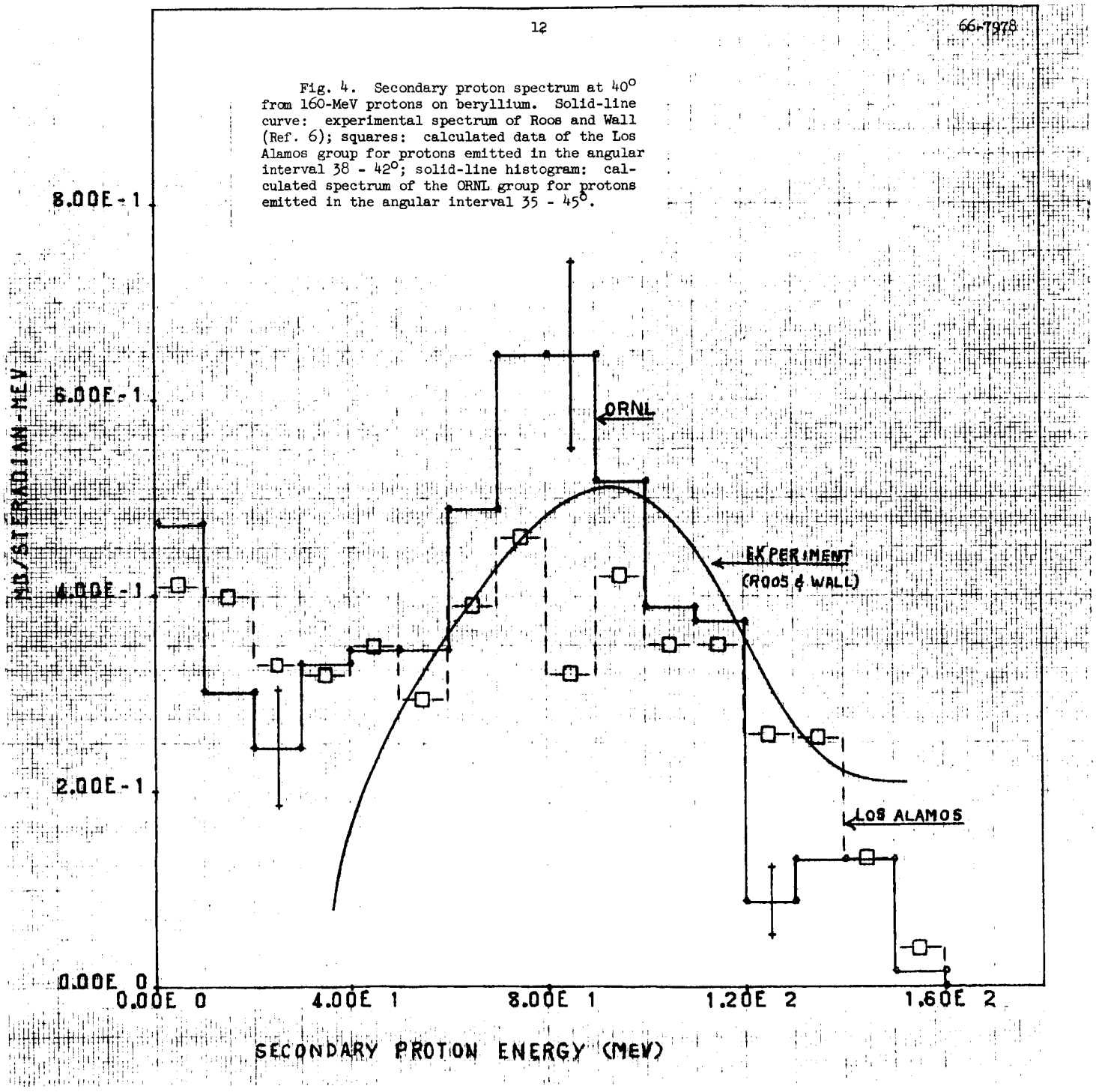

Fig. 5. Secondary proton spectrum at 60° from 160-MeV protons on beryllium. Solid-line curve: experimental spectrum of Roos and Wall (Ref. 6); squares: calculated data of the Los Alamos group for protons emitted in the angular interval 57 - 63°; solid-line histogram: calculated spectrum of the ORNL group for protons emitted in the angular interval 50 - 70°.

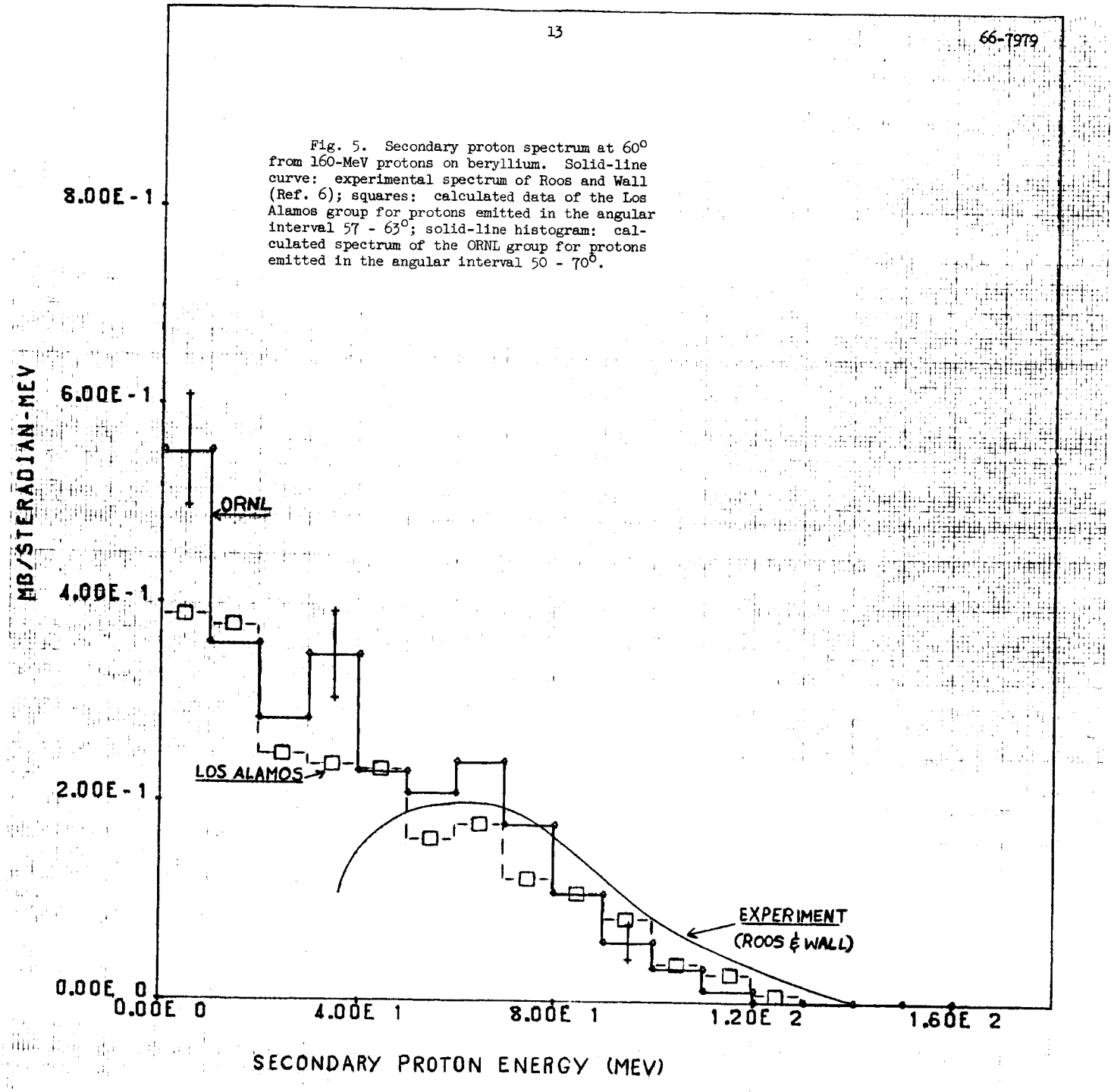

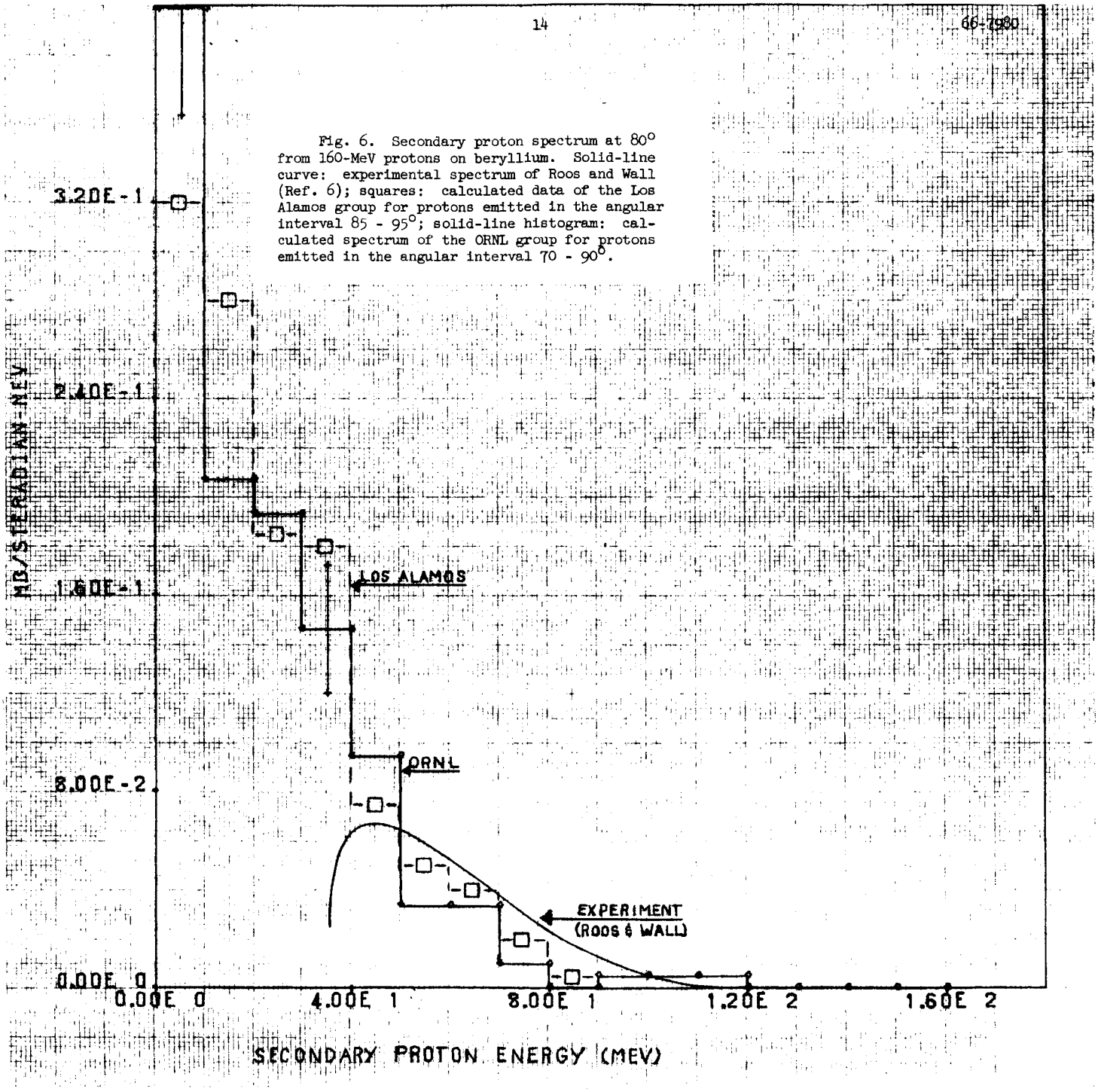

Fig. 6. Secondary proton spectrum at 80° from 160-MeV protons on beryllium. Solid-line curve: experimental spectrum of Roos and Wall (Ref. 6); squares: calculated data of the Los Alamos group for protons emitted in the angular interval 85 - 95°; solid-line histogram: calculated spectrum of the ORNL group for protons emitted in the angular interval 70 - 90°.

The proton spectra at various angles from 160-MeV protons on aluminum are illustrated in Figs. 7-10 for the ORNL and Brookhaven calculations and the experimental data of Peelle et al.[7] The calculations are in reasonable agreement with each other at all angles. There is also good agreement with the experimental results at all angles except 30°. However, the energy resolution of the experiments was not stringent enough to detect the peaks predicted by the calculations at 30°, but even without this, the agreement is fair.

Figs. 11-18 contain samples of everything. The proton spectra at various angles from 160-MeV protons on cobalt are illustrated. Comparisons between the Los Alamos and ORNL results are illustrated in Figs. 11, 12, 13, and 18. The greatest discrepancy between the two calculations is at 20°, Fig. 11, where a peak from the Los Alamos results lies between 110 and 120 MeV while that from the ORNL results lies between 130 and 140. A larger "quasi-elastic" peak is predicted by the Los Alamos calculation. At 40°, Fig. 12, the differences between the two results is fairly minor. An eye-ball comparison of the two calculated results with experiment would give Los Alamos the edge. At 60° and 80°, Figs. 18 and 13, the calculated results are essentially the same.

Figs. 14, 15, 16, and 17 are quite interesting because they contain the results of the Brookhaven calculations that were done with and without considering the effects of reflection and refraction. The effect of reflection and refraction at 30° and 45° (Figs. 14 and 15) is to suppress the quasi-elastic peak, but in doing so the number of particles escaping at these energies is reduced to the point where they are significantly different from the number predicted by the experiments. At these angles, the Brookhaven

B

Fig. 7. Secondary proton spectrum at 30° from 160-MeV protons on aluminum. Crossed error bars: experimental data of Peelle et al. (Ref. 7); circles: calculated data of the Brookhaven group for protons emitted in the angular interval 26 - 37° where reflection and refraction are included in the calculation; solid-line histogram: calculated spectrum of the ORNL group for protons emitted in the angular interval 20 - 40°.

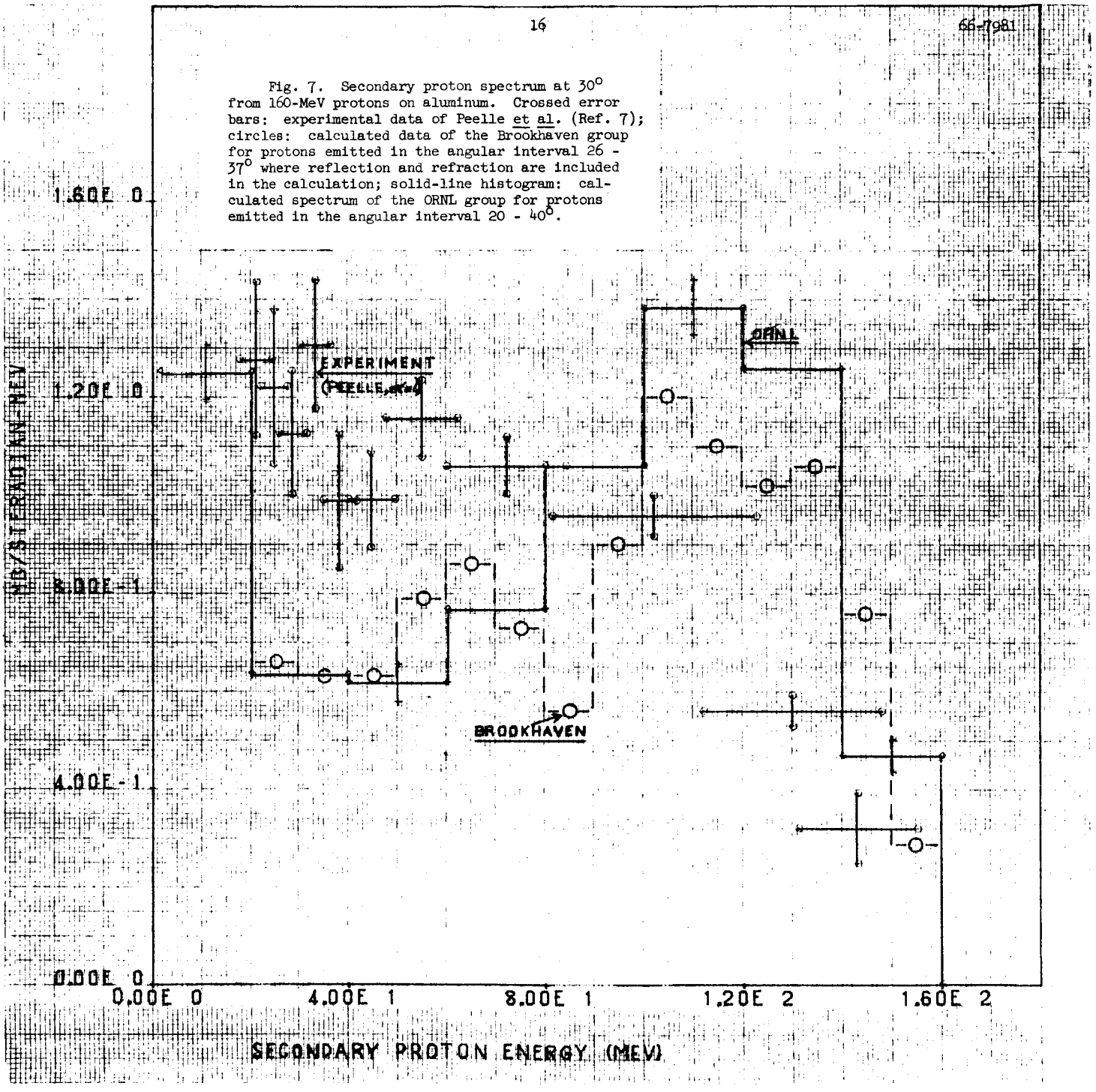

Fig. 8. Secondary proton spectrum at 45° from 160-MeV protons on aluminum. Crossed error bars: experimental data of Peelle et al. (Ref. 7); circles: calculated data of the Brookhaven group for protons emitted in the angular interval 37 - 53° where reflection and refraction are included in the calculation; solid-line histogram: calculated spectrum of the ORNL group for protons emitted in the angular interval 35 - 55°.

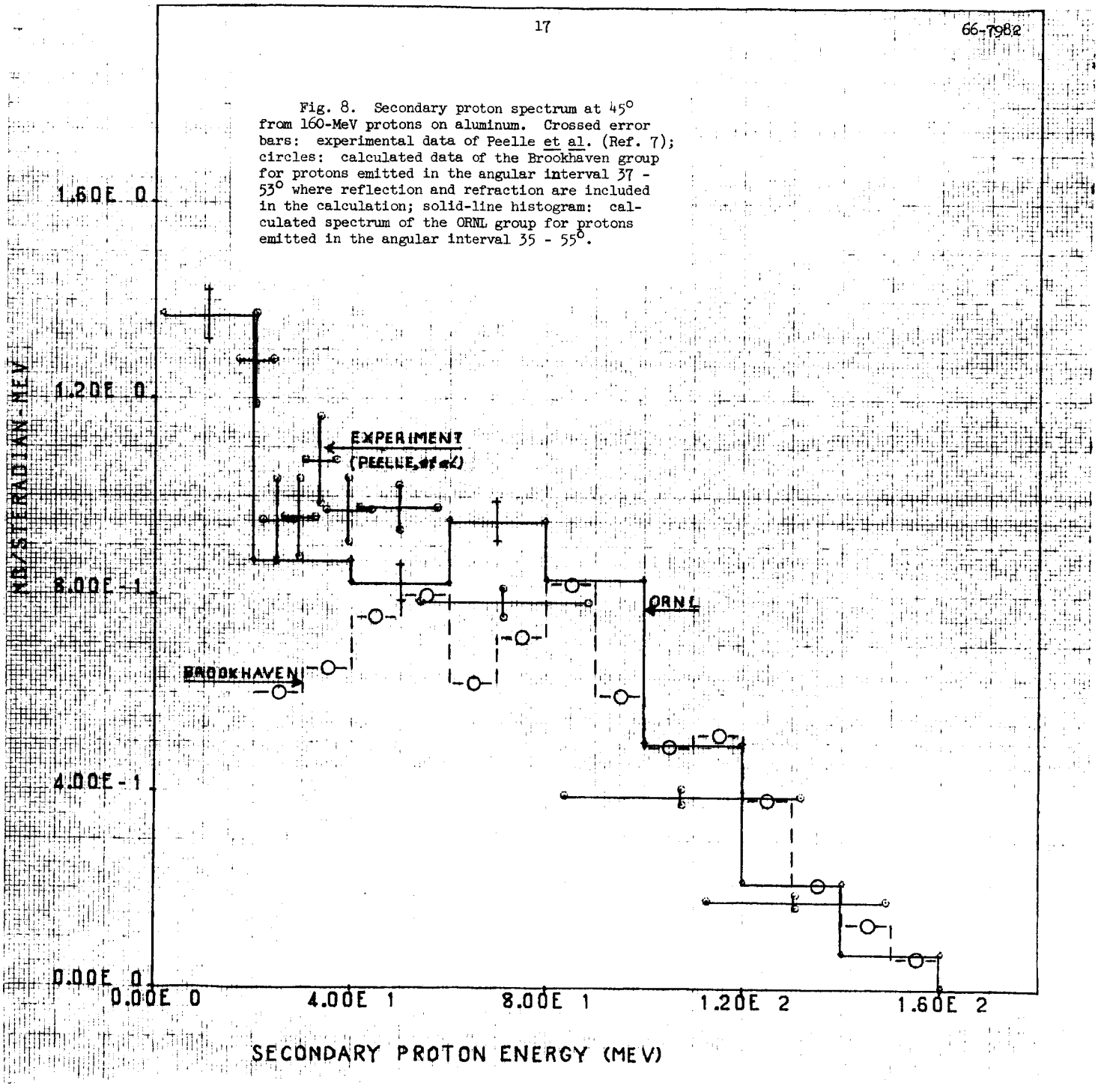

Fig. 9. Secondary proton spectrum at 60° from 160-MeV protons on aluminum. Crossed error bars: experimental data of Peelle et al. (Ref. 7); circles: calculated data of the Brookhaven group for protons emitted in the angular interval 53 - 66° where reflection and refraction are included in the calculation; solid-line histogram: calculated spectrum of the ORNL group for protons emitted in the angular interval 50 - 70°.

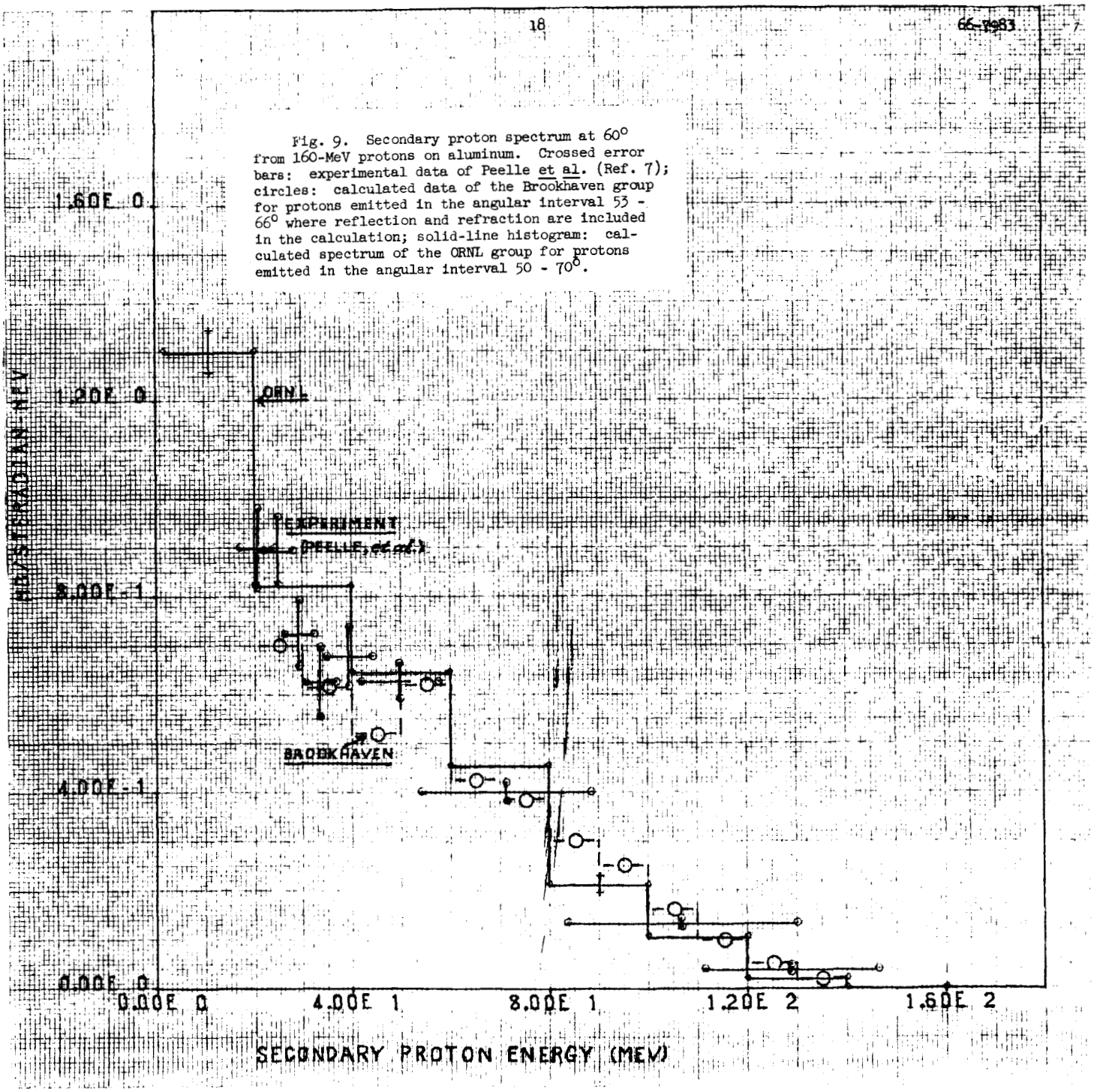

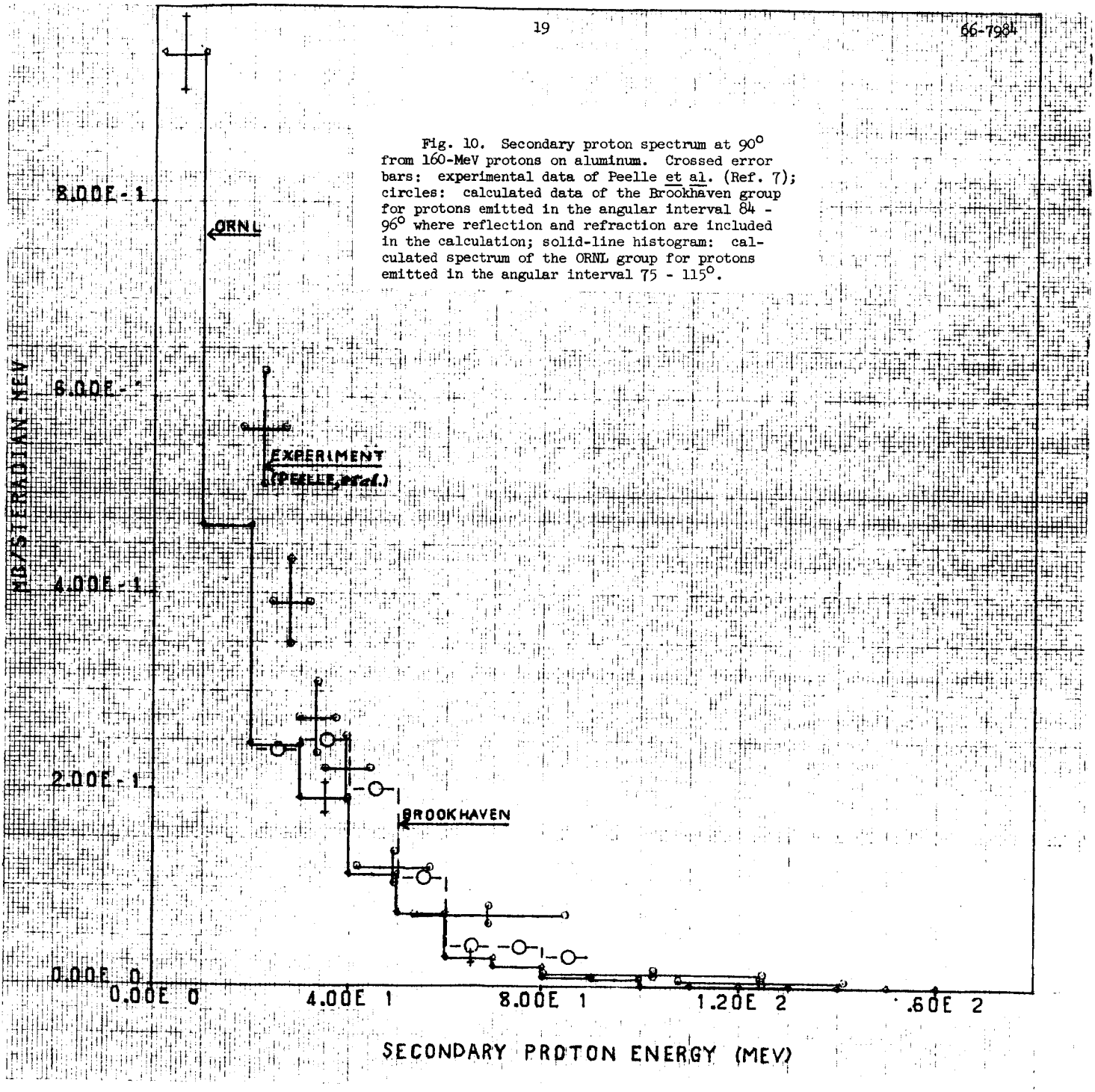

Fig. 10. Secondary proton spectrum at 90° from 160-MeV protons on aluminum. Crossed error bars: experimental data of Peelle et al. (Ref. 7); circles: calculated data of the Brookhaven group for protons emitted in the angular interval 84 - 96° where reflection and refraction are included in the calculation; solid-line histogram: calculated spectrum of the ORNL group for protons emitted in the angular interval 75 - 115°.

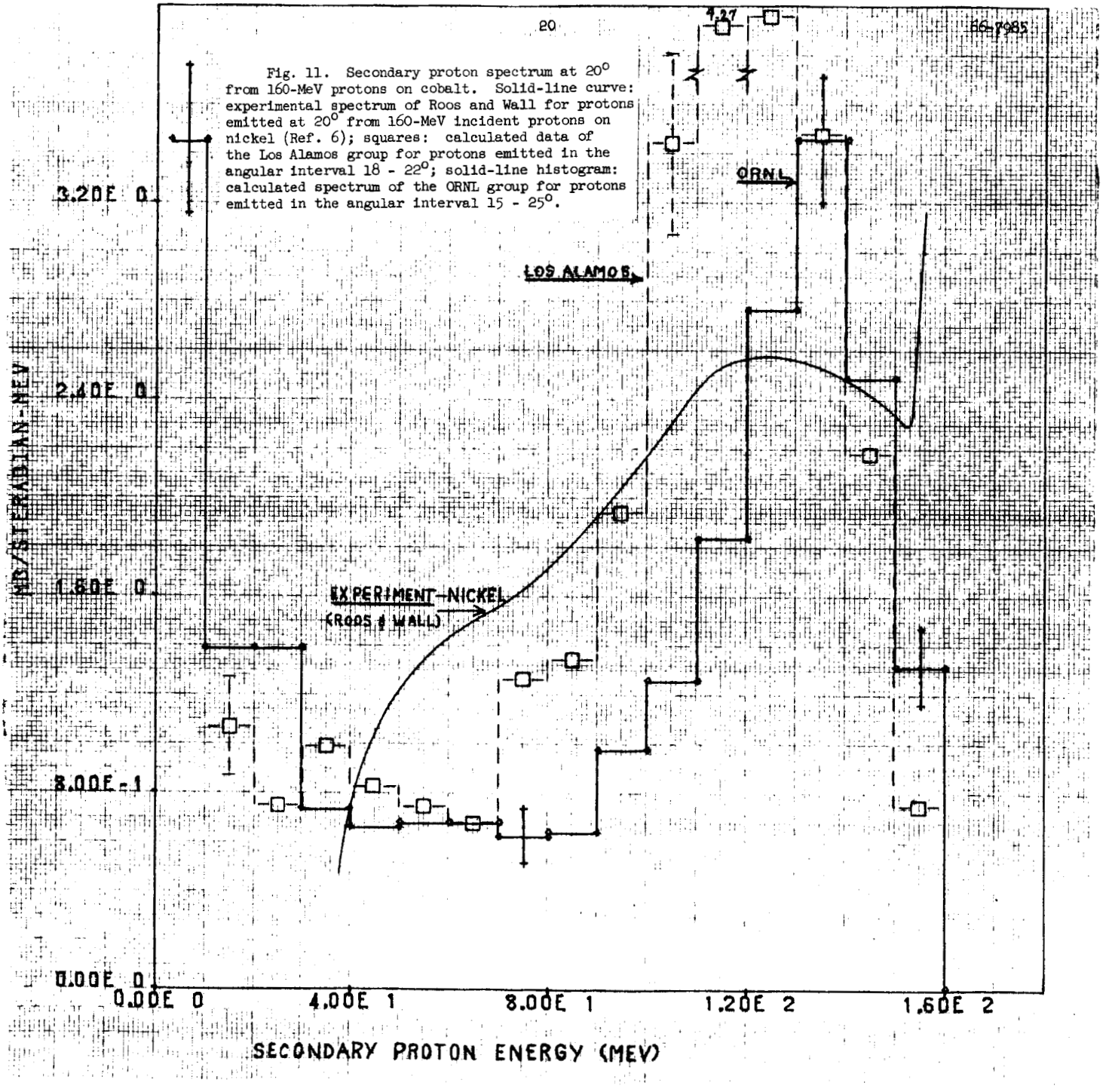

Fig. 11. Secondary proton spectrum at 20° from 160-MeV protons on cobalt. Solid-line curve: experimental spectrum of Roos and Wall for protons emitted at 20° from 160-MeV incident protons on nickel (Ref. 6); squares: calculated data of the Los Alamos group for protons emitted in the angular interval 18 - 22°; solid-line histogram: calculated spectrum of the ORNL group for protons emitted in the angular interval 15 - 25°.

Fig. 12. Secondary proton spectrum at 40° from 160-MeV protons on cobalt. Solid-line curve: experimental spectrum of Roos and Wall for protons emitted at 40° from 160-MeV incident protons on nickel (Ref. 6); squares: calculated data of the Los Alamos group for protons emitted in the angular interval 38 - 42°; solid-line histogram: calculated spectrum of the ORNL group for protons emitted in the angular interval 35 - 45°.

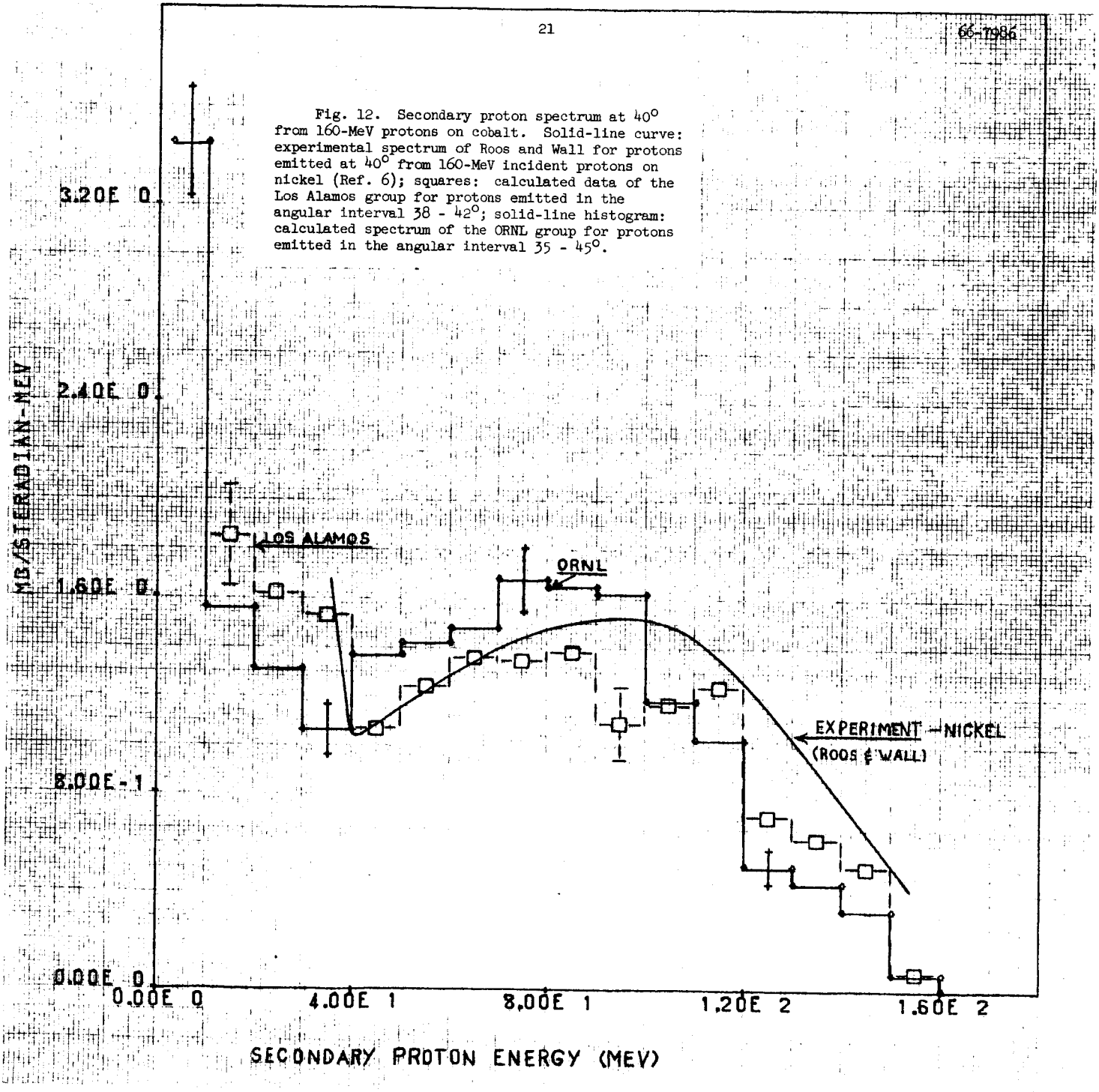

Fig. 13. Secondary proton spectrum at 80° from 160-MeV protons on cobalt. Solid-line curve: experimental spectrum of Roos and Wall for protons emitted at 80° from 160-MeV incident protons on nickel (Ref. 6); squares: calculated data of the Los Alamos group for protons emitted in the angular interval 78 - 82°; solid-line histogram: calculated spectrum of the ORNL group for protons emitted in the angular interval 70 - 90°.

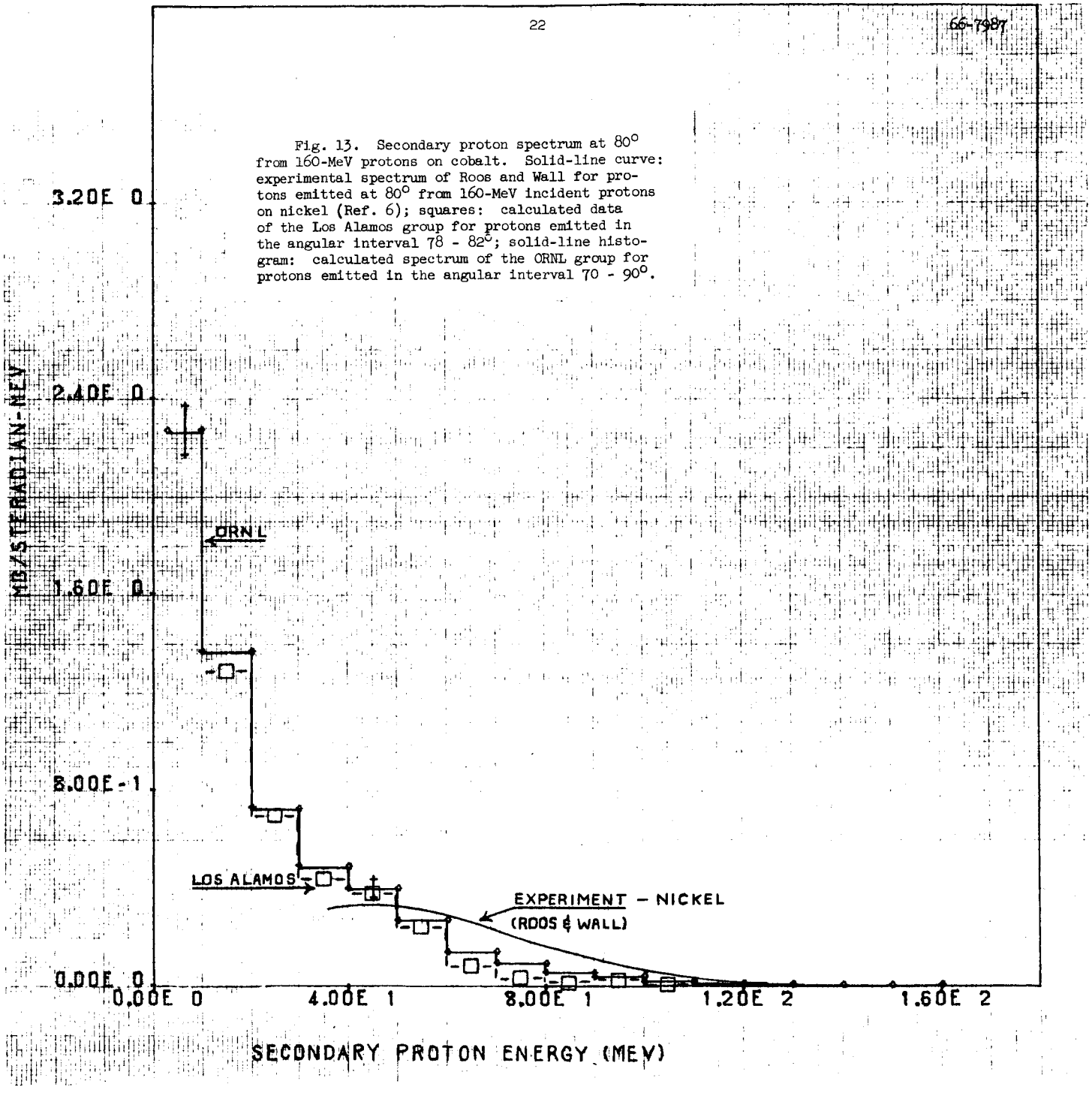

Fig. 14. Secondary proton spectrum at 30° from 160-MeV protons on cobalt. Crossed error bars: experimental data of Peelle et al. (Ref. 7); circles (with reflection and refraction) and X's (without reflection and refraction): calculated data of the Brookhaven group for protons emitted in the angular interval 26 - 37°; solid-line histogram: calculated spectrum of the ORNL group for protons emitted in the angular interval 20 - 40°.

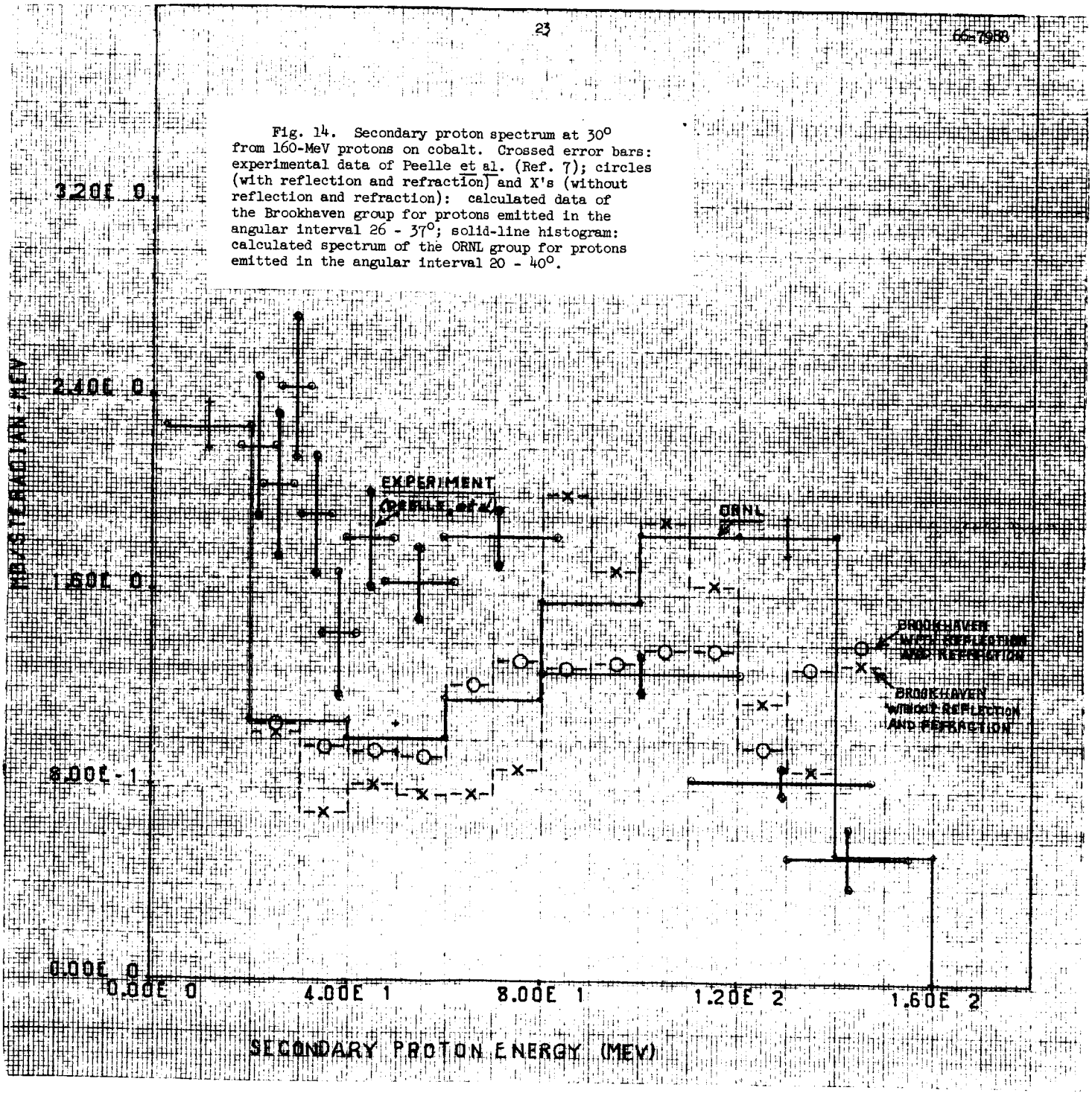

Fig. 15. Secondary proton spectrum at 45° from 160-MeV protons on cobalt. Crossed error bars: experimental data of Peelle et al. (Ref. 7); circles (with reflection and refraction) and X's (without reflection and refraction): calculated data of the Brookhaven group for protons emitted in the angular interval 37 - 53°; solid-line histogram: calculated spectrum of the ORNL group for protons emitted in the angular interval 35 - 55°.

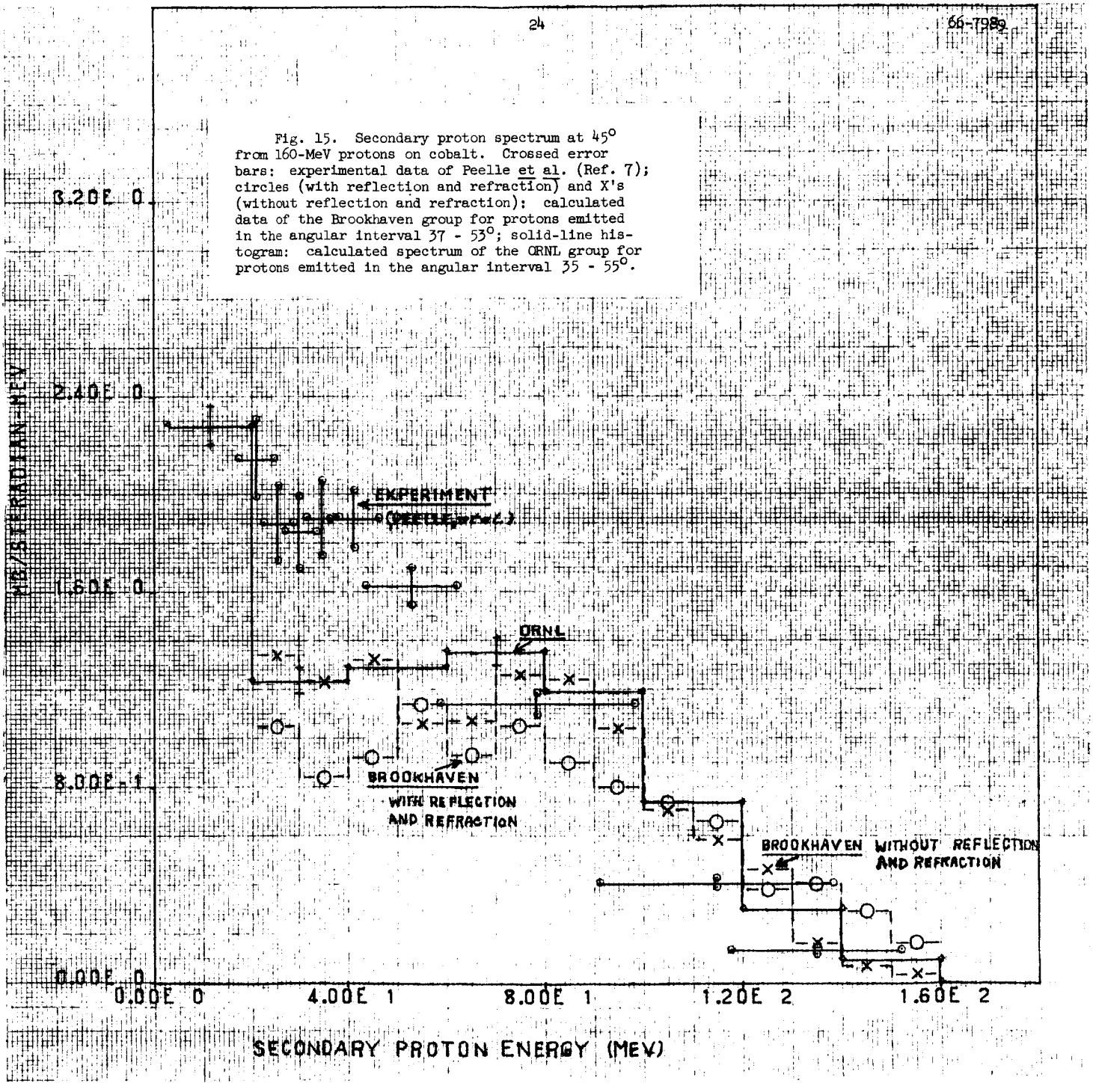

Fig. 16. Secondary proton spectrum at 90° from 160-MeV protons on cobalt. Crossed error bars: experimental data of Peelle et al. (Ref. 7); circles (with reflection and refraction) and X's (without reflection and refraction): calculated data of the Brookhaven group for protons emitted in the angular interval 84 - 96°; solid-line histogram: calculated spectrum of the ORNL group for protons emitted in the angular interval 75 - 115°.

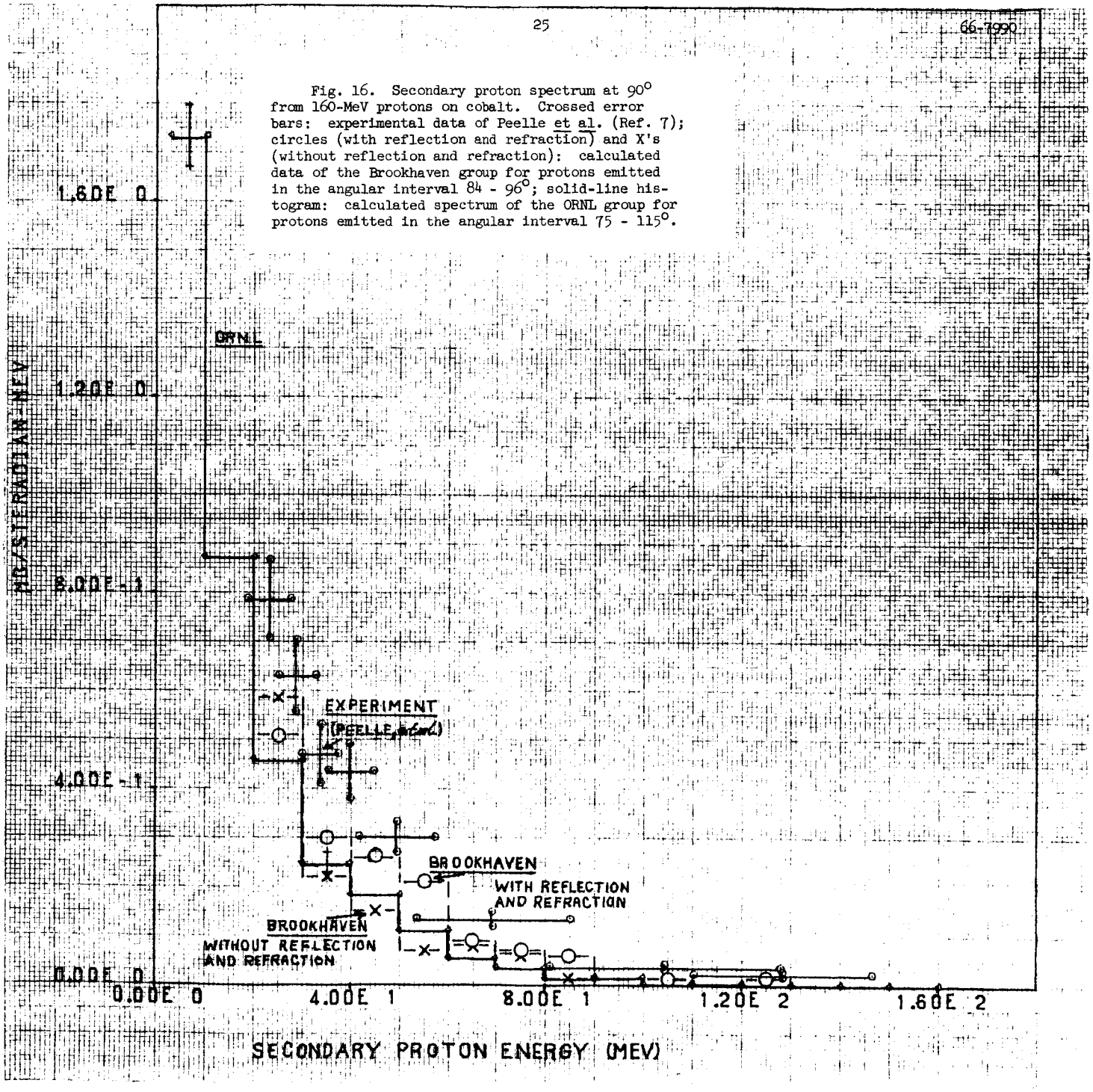

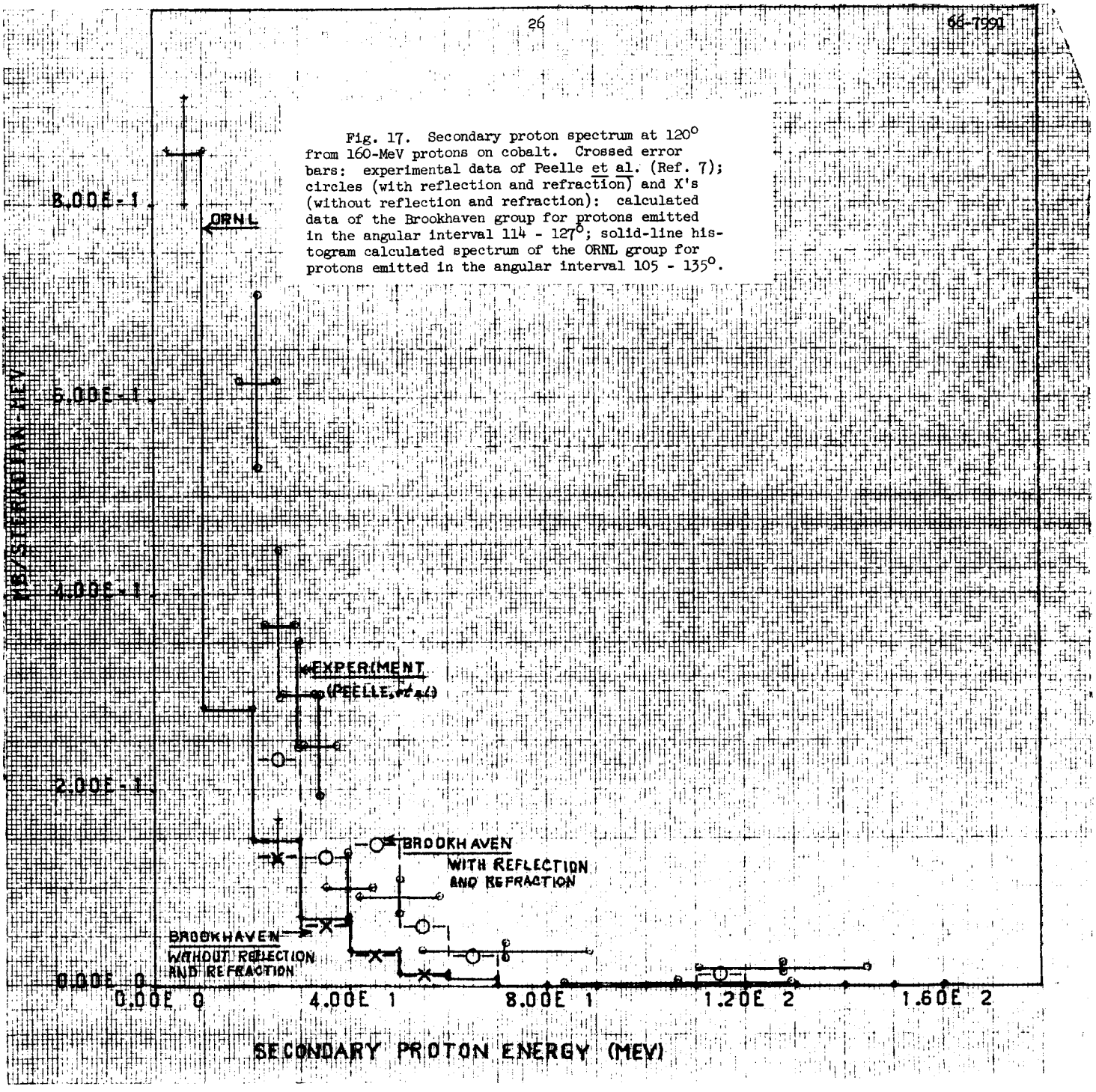

Fig. 17. Secondary proton spectrum at 120° from 160-MeV protons on cobalt. Crossed error bars: experimental data of Peelle et al. (Ref. 7); circles (with reflection and refraction) and X's (without reflection and refraction): calculated data of the Brookhaven group for protons emitted in the angular interval 114 - 127°; solid-line histogram calculated spectrum of the ORNL group for protons emitted in the angular interval 105 - 135°.

Fig. 18. Secondary proton spectrum at 60° from 160-MeV protons on cobalt. Crossed error bars: experimental data of Peelle et al. (Ref. 7); solid-line curve: experimental spectrum of Roos and Wall for protons emitted at 60° from 160-MeV incident protons on nickel (Ref. 6); squares: calculated data of the Los Alamos group for protons emitted in the angular interval 58 - 62°; circles: calculated data of the Brookhaven group for protons emitted in the angular interval 53 - 66° where reflection and refraction are included in the calculation; solid-line histogram: calculated spectrum of the ORNL group for protons emitted in the angular interval 50 - 70°.

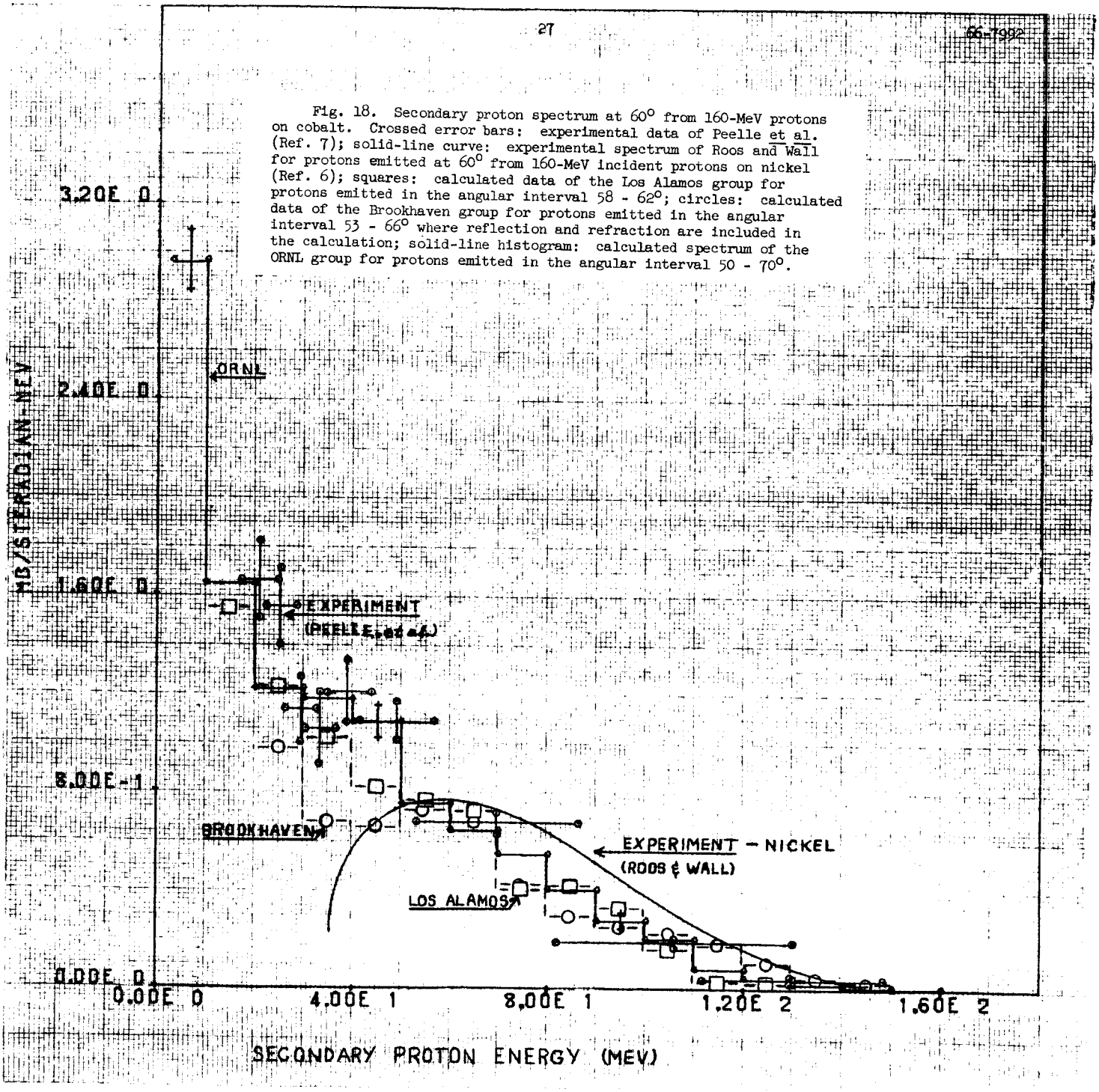

calculation without refraction compares well with the ORNL calculation. The poor high energy resolution of the experiments makes it difficult to make a statement about the agreement with experiment, particularly at 30°. One does see a peak at 20° and 40° (Figs. 11 and 12) from other experimental data,[6] which lends credence to the predicted shape of the spectrum from the ORNL and Brookhaven (without reflection) calculation.

At 90° and 120° (Figs. 16 and 17) the Brookhaven calculation without reflection and refraction and the ORNL calculations yield results which are almost identical. The magnitude of these spectra, however, are noticeably lower than the experimental spectra. Here the Brookhaven calculation that includes reflection and refraction yields results which are more consistent with the experiments.

With the exception of the low energy part of the Roos and Wall[6] data, all of the data are in reasonable agreement for the spectra at 60° which are illustrated in Fig. 18.

The proton spectra at 30° from 160-MeV protons on a heavy element, bismuth, are illustrated in Fig. 19. The ORNL calculations yield a quasi-elastic peak, while the Brookhaven calculation that includes reflection and refraction and the experiments give no indication of a peak. The most troublesome disagreement between both sets of calculations and the experiment is that the number of particles emitted at this angle is underestimated by both sets of calculations.

There will be no attempt made to summarize all of the results presented here.

Fig. 19. Secondary proton spectrum at 30° from 160-MeV protons on bismuth. Crossed error bars: experimental data of Peelle et al. (Ref. 7); circles: calculated data of the Brookhaven group for protons emitted in the angular interval 26 - 37° where refraction and reflection are included in the calculation; solid-line histogram: calculated spectrum of the ORNL group for protons emitted in the angular interval 20 - 40°.

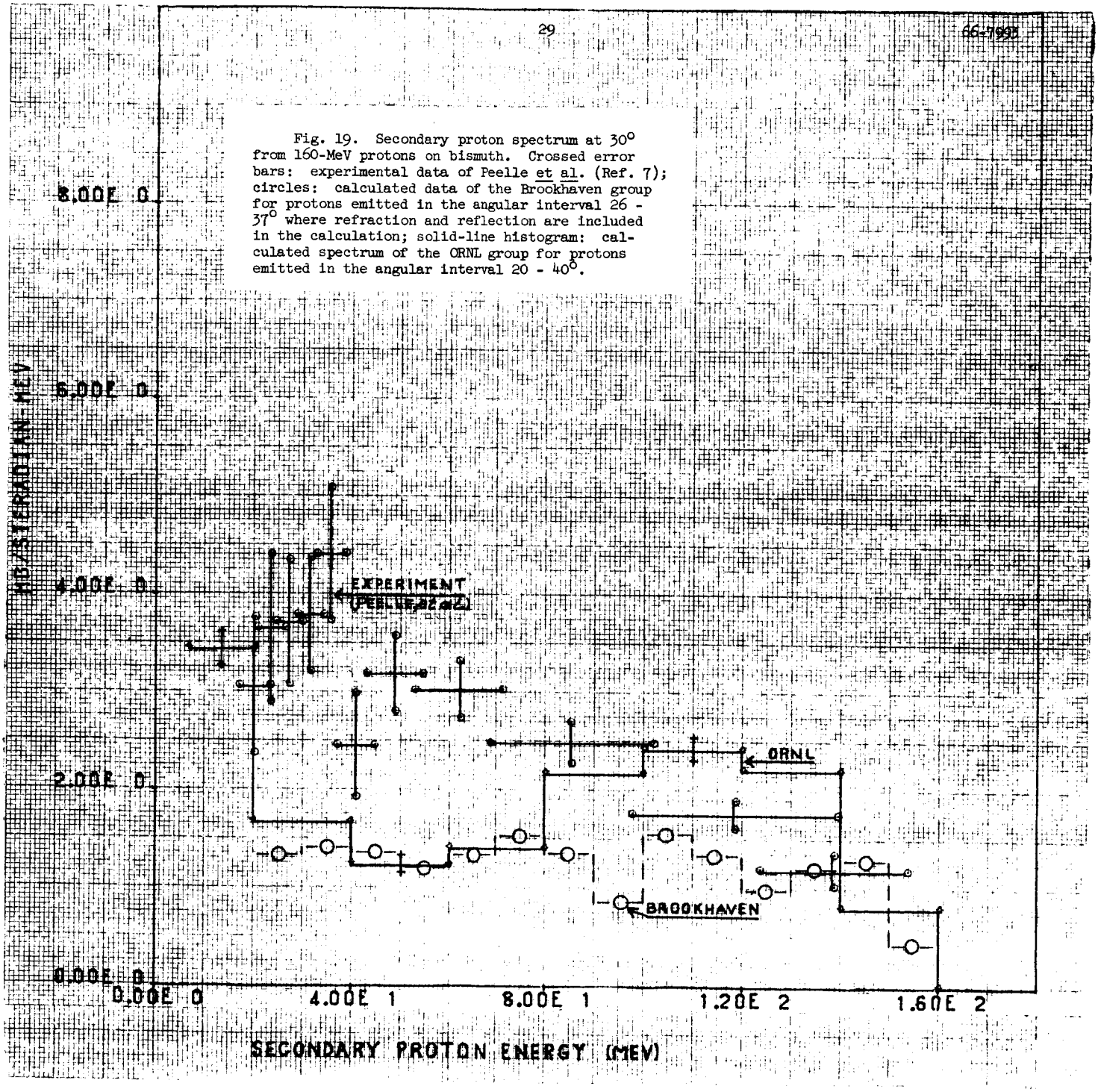

VI. ACKNOWLEDGMENT

The author has had contact with all of the people working on the other calculations. However, he has conversed more with J. M. Miller, of Columbia, and D. R. Cochran, of Los Alamos, and greatly appreciates their willingness to discuss some of our problems and the sending of their preliminary data, which are illustrated here.

REFERENCES

1. Hugo W. Bertini, Phys. Rev. 131, 1801 (1963) with erratum Phys. Rev. 138, AB2 (1965)

2. R. Hofstadter, Rev. Mod. Phys. 28, 214 (1956)

3. C. D. Zerby, R. B. Curtis, H. W. Bertini, The Relativistic Doppler Problem ORNL-CF-61-7-20 (July 12, 1961)

4. Metropolis, Bivins, Storm, Turkevich, and Friedlander, Phys. Rev. 110, 185 (1958)

5. P. H. Bowen, G. C. Cox, G. B. Huxtable, J. P. Scanlon, J. J. Thresher, and A. Langsford, Nuclear Phys. 30, 475 (1962)

6. P. G. Roos, Elastic and Inelastic Scattering of High Energy Protons from Nuclei, University of Maryland, College Park, Maryland, Dept. of Physics and Astronomy, Sept. 1964; a dissertation under the supervision of N. S. Wall.

7. R. W. Peelle, T. A. Love, N. W. Hill, and R. T. Santoro, Neutron Phys. Div. Ann. Progr. Rept. Aug. 1, 1964, ORNL-3714, Vol. 2, p. 120

DO NOT PRINT

INTERNAL DISTRIBUTION

1-2. L. S. Abbott
3. F. S. Alsmiller
4. R. G. Alsmiller, Jr.
5-34. H. W. Bertini
35. W. R. Burrus
36. W. Coleman
37. W. A. Gibson
38. M. P. Guthrie
39. D. C. Irving
40. T. A. Love
41. F. C. Maienschein
42. R. W. Peelle
43. R. T. Santoro
44. V. V. Verbinski
45. J. W. Wachter
46. W. Zobel
47. G. Dessauer (Consultant)
48. B. C. Diven (Consultant)
49. M. L. Goldberger (Consultant)
50. M. H. Kalos (Consultant)
51. L. V. Spencer (Consultant)
52-53. Central Research Library
54-55. Y-12 Document Reference Section
56-60. Laboratory Records
61. Laboratory Records ORNL RC
62. ORNL Patent Office

EXTERNAL DISTRIBUTION

63-72. D. R. Cochran, Los Alamos Scientific Laboratory, Los Alamos, New Mexico
73. J. W. Keller, NASA Headquarters, Washington, D. C.
74. D. T. King, University of Tennessee, Knoxville, Tennessee
75-84. J. H. Miller, Columbia University, New York, New York
85. A. Reetz, NASA Headquarters, Washington, D. C.